# OBSTACLE AVOIDING STRATEGY OF A RECONFIGURABLE REDUNDANT SPACE ROBOT

**Vijay Kumar Dalla[(a)], Pushparaj Mani Pathak[(b)],**

[(a),(b)] Mechanical and Industrial Engineering Department
Indian Institute of Technology, Roorkee
Roorkee-247667, India

[(a)]vijaydalla@gmail.com, [(b)]pushpfme@iitr.ac.in

**ABSTRACT**

This paper presents a strategy for collision-free robot tip trajectory in space works. Obstacles present in the workspace may collide with a space robotic system engaged in on-orbital servicing missions. The resultant collision may damage to the manipulator which ultimately leads to the space mission failure. When a space robot needs to perform in a limited volume with obstacles present, the robot must possess some unique capability to reach around obstacles during maneuvering. The redundant robot can perform various tasks in a limited workspace with obstacles. Hence, for this, a 6DOF space robot has been proposed for manipulation in the workspace with two static obstacles. Collision avoidance is based on reconfiguration approach where the joints are made active/passive to facilitate collision-free tip trajectory. Before reconfiguration, collision detection has been proposed to be done. The bond graph technique has been used for the dynamic model of the system and to formulate system equations.

Keywords: redundant space robot, collision avoidance, trajectory planning, bond graph modeling.

## 1. INTRODUCTION

Redundant manipulator (Agrawal 1994; Sutar et al. 2015) refers to a kind of robot which possesses additional degree of freedom than required to perform the desired tasks. Among various task execution capabilities (Sardana et al. 2013) of a redundant robot, obstacle avoidance characteristics have its own significant because if the robot collides with the obstacles, both the robot and the obstacles may get damages. The collision free trajectory has two folds: robot tip motion planning known as main task and the robot link collision avoidance known as sub-task. The tip motion planning is needed when the obstacles are located in the workspace. The dynamic motion planning of the space robot is itself a complex task due to its floating base and has been paying considerable attention during the last years (Pathak et al. 2006; Saha 1996; Shah et al. 2013). Obstacle avoidance (Dasgupta et al. 2009; Singla et al. 2010) is a further additional difficulty.

Most of the previous researches have only focused on industrial and mobile manipulators. Some of them are discussed here as: Usually, strategies of collision free trajectory are based on Artificial Potential Field (Csiszar et al. 2012) by imposing repulsive and attractive forces, where the sources are the obstacles and the target, respectively. In which, the robot is repulsed away from the obstacles (static and dynamic) and is attracted to the target position. This method is simple and has elegant mathematics. Some inherent weaknesses are studied by (Koren and Borenstein 1999). (Bjerkeng et al. 2011) discussed a novel approach for collision-free tip motion for industrial manipulators based on the weighted pseudo inverse kinematic redundancy resolution technique (Whitne 1969). To use the pseudo inverse control approach is a big challenge due to the requirement of a well behaved task parameterization. The inherent limitations of the weighted pseudo inverse are discussed in (Klein et al. 1983). A nonholonomic mobile robot was presented for trajectory tracking with obstacle avoidance based on an analytical method (Korayem et al. 2014). The limitation of this method is that the generated path solution was parameterized to a limited fixed-order polynomial.

Most of the earlier works on collision avoidance are based on an optimization approaches. These approaches have their inherent limitations such as one does not have any information about the manipulator configuration after collision-avoidance. In a work (Shari and Troch 1996), based on reconfiguration approach, one can know the final configuration, i.e., configuration after obstacles avoidance which can be influenced by further requirements such as joint limit, singularity avoidance, etc. For behavior based control strategy, a fuzzy method has been developed for obstacle avoidance of multi-link manipulator (Dassanayake et al. 1999). Using this method, there is no need to evaluate inverse kinematics.

Still, a few literatures discuss about collision free trajectories in space. A practical 3-D seven DOF redundant manipulator was taken for collision-free trajectory planning (Mu et al. 2014) based on pseudo-distance. The natures of obstacles were both static and

dynamics. To plan a 3-D trajectory planning with collision avoidance, gradient projection was presented. This method provides high computation efficiency and good real time due to avoidance of complex computation of Euclidean distance. These aforementioned literatures motivated us to utilize unconventional features of the redundant space robot for collision-free trajectory planning.

In our work, 6 DOF space robot has been proposed for safe trajectory tracking with static environments. The static environments include two obstacles in the workspace. This work is based on reconfiguration approach. Among 6 joints only two joints are supposed to be actuated at a time, whereas others are kept passive. However, every joint can be actuated but some of them will not for the kinematic control purpose. When a link comes close to the obstacles, the joint of the respective/influencing link is made passive and in between other passive is released to be actuated and then the manipulator is reconfigured. In this way, by exploiting redundancy, a collision-free trajectory can be achieved. It is worth mentioning that each joint is controlled independently by using Proportional-Derivative controller. The end-effector trajectory tracking is taken care by using Proportional-Integral-Derivative controller.

This paper is organized in 6 sections. Section 2 presents a physical model of 6 DOF planar space robots. Section 3 discusses about recognition of obstacles present in the workspace. Section 4 deals the simulation and the animation results. Finally, section 6 presents conclusions.

## 2. MODEL OF 6DOF PLANAR SPACE ROBOTIC SYSTEM

This section discusses about the entire procedure of development of a dynamic model of 6 DOF planar space robot. Modeling of the 6DOF planar space robot involves translational and rotational dynamics of the links. The basis of modeling depends upon assumptions that the robot base and all the links are rigid body. Also, the joints are assumed to be revolute joints and the robot has a single arm and it is an open kinematic chain. Figure 1 represents a schematic sketch of the 6 DOF planar space robot. In this Figure, {*A*} is the inertial or absolute frame and {*V*} is the vehicle frame located at the center of mass (CM) of the space robot. A frame {0} is located on space robot base at the root of the manipulator of space robot. Frame {1} is also located at the root of manipulator at the first joint. Frames {2} to {6} are attached at the joints 2 to 6 of the manipulator, respectively. Frame {7} is located at the tip of the manipulator or at the end effector of the space robot. Let, *r* is the distance between the vehicle frame and the root of the robot frame. Let, $l_1$ to $l_6$ are the length of the links 1 to 6 of the manipulator, respectively.

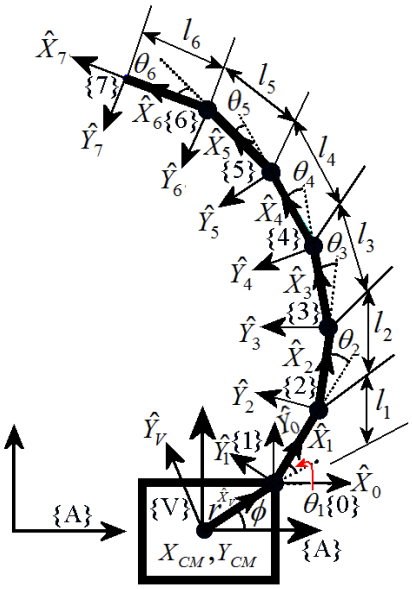


Figure 1. Schematic Sketch of 6DOF Planar Space Robot System

Let $\phi$ represents the rotation of the frame {*V*} with respect to the frame {*A*}. Let $\theta_1$ to $\theta_6$ show 1st to 6th joint angles of the manipulator, respectively. Let $X_{CM,}$ and $Y_{CM}$ denote the center of mass (CM) of the robot base with respect to the absolute frame {*A*}. Kinematic relations are expressed in terms of the tip position and orientation as:

$$X_{tip} = X_{CM} + rc(\phi) + l_1 c(\theta_{\phi 1}) + l_2 c(\theta_{\phi 12}) + l_3 c(\theta_{\phi 123}) + l_4 c(\theta_{\phi 1234}) + l_5 c(\theta_{\phi 12345}) + l_6 c(\theta_{\phi 123456}) \quad (1)$$

$$Y_{tip} = Y_{CM} + r\, s(\phi) + l_1\, s(\theta_{\phi 1}) + l_2 s(\theta_{\phi 12}) + l_3 s(\theta_{\phi 123}) + l_4 s(\theta_{\phi 1234}) + l_5 s(\theta_{\phi 12345}) + l_6 s(\theta_{\phi 123456}) \quad (2)$$

$$\theta_{\phi 1} = \phi + \theta_1, \theta_{\phi 12} = \theta_{\phi 1} + \theta_2, \theta_{\phi 123} = \theta_{\phi 12} + \theta_3$$

Where, $\theta_{\phi 1234} = \theta_{\phi 123} + \theta_4, \theta_{\phi 12345} = \theta_{\phi 1234} + \theta_5,$

$$\theta_{\phi 123456} = \theta_{\phi 12345} + \theta_6.$$

$$\theta_{tip} = \theta_{\phi 123456} = \phi + \theta_1 + \theta_2 + \theta_3 + \theta_4 + \theta_5 + \theta_6 \quad (3)$$

Here, *s*( ) and *c*( ) represent sin( ) and cos( ), respectively. The tip translational and the angular velocities can be evaluated with help of Equations 1, 2 and 3 as,

$$\dot{X}_{tip} = \dot{X}_{CM} - r\dot{\phi}s(\phi) - l_1(\dot{\theta}_{\phi 1})s(\theta_{\phi 1}) - l_2(\dot{\theta}_{\phi 12})s(\theta_{\phi 2}) - l_3(\dot{\theta}_{\phi 123})s(\theta_{\phi 123}) - l_4(\dot{\theta}_{\phi 1234})s(\theta_{\phi 1234}) - l_5(\dot{\theta}_{\phi 12345})s(\theta_{\phi 12345}) - l_6(\dot{\theta}_{\phi 123456})s(\theta_{\phi 123456}) \quad (4)$$

$$\dot{Y}_{tip} = \dot{X}_{CM} + r\dot{\phi}c(\phi) + l_1(\dot{\theta}_{\phi 1})c(\theta_{\phi 1}) + l_2(\dot{\theta}_{\phi 12})c(\theta_{\phi 2}) + l_3(\dot{\theta}_{\phi 123})c(\theta_{\phi 123}) + l_4(\dot{\theta}_{\phi 1234})c(\theta_{\phi 1234}) + l_5(\dot{\theta}_{\phi 12345})c(\theta_{\phi 12345}) + l_6(\dot{\theta}_{\phi 123456})c(\theta_{\phi 123456}) \quad (5)$$

$$\dot{\theta}_{tip} = \dot{\theta}_{\phi 123456} = \dot{\phi} + \dot{\theta}_1 + \dot{\theta}_2 + \dot{\theta}_3 + \dot{\theta}_4 + \dot{\theta}_5 + \dot{\theta}_6 \quad (6)$$

Since we will not actuate all joints simultaneously for the kinematic control purpose, the robot needs to be reconfigured. Suppose, initially joints 1 and 4 are active and the rest are passive joints. Figure 2 consists of the original configuration of 6DOF robot and the reconfigured robot. In this case, where, joint 1 and joint 4 are actuated, the kinematic relations for the tip displacements $X^{\#}_{tip}$ and $Y^{\#}_{tip}$ in $X$ and $Y$ directions can be derived as,

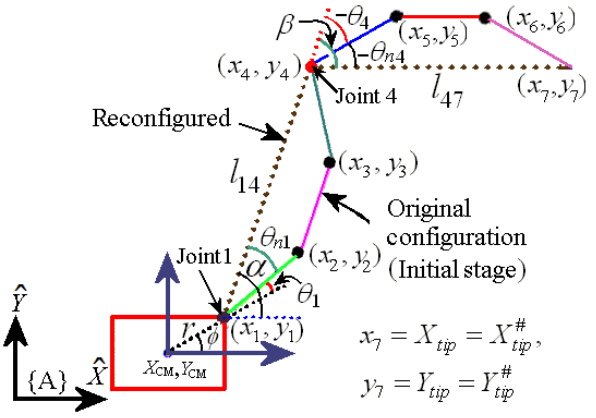


Figure 2. Schematic Sketch of the Original Configuration of 6DOF Robot and the Reconfigured Robot

$$X^{\#}_{tip} = X_{CM} + rc(\phi) + l_{14}c(\alpha) + l_{47}c(\beta) \quad (7)$$

$$Y^{\#}_{tip} = Y_{CM} + rs(\phi) + l_{14}s(\alpha) + l_{47}s(\beta) \quad (8)$$

$$\text{Where, } \begin{matrix} \alpha = \phi + \theta_1 + \theta_{n1} = \phi + \theta_{1n1}, \\ \beta = \alpha - \theta_4 - \theta_{n4} = \alpha - \theta_{4n4}. \end{matrix} \quad (9)$$

Here, $\theta_{n1}$ and $\theta_{n4}$ are unknown, hence, $\alpha$ and $\beta$ become unknown.

$$l_{14} = \sqrt{(x_4 - x_1)^2 + (y_4 - y_1)^2}, \quad l_{47} = \sqrt{(x_7 - x_4)^2 + (y_7 - y_4)^2} \quad (10)$$

The variables used in the Equation 10 can be evaluated from the original configuration (Fig. 2) as,

$$x_1 = X_{CM} + rc(\phi) \quad (11)$$

$$y_1 = Y_{CM} + rs(\phi) \quad (12)$$

$$x_4 = X_{CM} + rc(\phi) + l_1c(\theta_{\phi 1}) + l_2c(\theta_{\phi 12}) + l_3c(\theta_{\phi 123}) \quad (13)$$

$$y_4 = Y_{CM} + r\,s(\phi) + l_1\,s(\theta_{\phi 1}) + l_2s(\theta_{\phi 12}) + l_3s(\theta_{\phi 123}) \quad (14)$$

$x_7 = X_{tip}, y_7 = Y_{tip}$ where, $X_{tip}$ and $Y_{tip}$ are evaluated from Equations 1 and 2.

Now, the unknown joint variables $\alpha$ and $\beta$ of Equations 7 and 8, need to be calculated.

For reconfigured robot, $x_4$ and $y_4$ of Equations 13 and 14 can also be expressed as,

$$x_4 = X_{CM} + rc(\phi) + l_{14}c(\alpha) \quad (15)$$

$$y_4 = Y_{CM} + rs(\phi) + l_{14}s(\alpha) \quad (16)$$

By equating Equation 13 with 15 and 14 with 16 and simplifying them, $\alpha$ is calculated as,

$$\alpha = \tan^{-1}[(l_1\,s(\theta_{\phi 1}) + l_2s(\theta_{\phi 12}) + l_3s(\theta_{\phi 123}))/(l_1c(\theta_{\phi 1}) + l_2c(\theta_{\phi 12}) + l_3c(\theta_{\phi 123}))] \quad (17)$$

Similarly, $\beta$ can be found by equating and simplifying the tips of 6DOF robot (original robot) and reconfigured robot (Fig. 2), i.e., Equation (7) with (1) and (8) with (2).

$$\beta = \tan^{-1}[\{l_1\,s(\theta_{\phi 1}) + l_2s(\theta_{\phi 12}) + l_3s(\theta_{\phi 123}) + l_4s(\theta_{\phi 1234}) + l_5s(\theta_{\phi 12345}) + l_6s(\theta_{\phi 123456}) - l_{14}s(\alpha)\}/\{l_1c(\theta_{\phi 1}) + l_2c(\theta_{\phi 12}) + l_3c(\theta_{\phi 123}) + l_4c(\theta_{\phi 1234}) + l_5c(\theta_{\phi 12345}) + l_6c(\theta_{\phi 123456}) - l_{14}c(\alpha)\}] \quad (18)$$

The tip velocity can be found by differentiating Equations 7 and 8 as,

$$\dot{X}^{\#}_{tip} = \dot{X}_{CM} - r(\dot{\phi})s(\phi) - l_{14}(\dot{\alpha})s(\alpha) - l_{47}(\dot{\beta})s(\beta) \quad (19)$$

$$\dot{Y}^{\#}_{tip} = \dot{Y}_{CM} + r(\dot{\phi})c(\phi) + l_{14}(\dot{\alpha})c(\alpha) + l_{47}(\dot{\beta})c(\beta) \quad (20)$$

Equations 19 and 20 help in evaluating transformer moduli (Table 1) for drawing bond graph model of the reconfigured space robot as shown in Figure 3. In Figure 3, *I* elements are used to model translational and rotational inertia of the space robot system. The *R* element represents the damping present at joints. The inertial element in the controller (Figure 4) is differentially causalled which is removed by adding a Soft Pad. The dynamic consequence of the Soft Pad

Table 1: TransformerModuli used in Bond Graph Model of the Reconfigured Space Robot

| Description | *X* -Direction | *Y* -Direction |
|---|---|---|
| Robot base | $\mu_2$: -*r* sin$\phi$ | $\mu_1$ : *r* cos$\phi$ |
| Reconfigured link 1-tip | $\mu_6$: -$l_{14}$ sin$\alpha$ | $\mu_5$:$l_{14}$ cos$\alpha$ |
| Reconfigured link 1-CM | $\mu_4$:-0.5 $l_{14}$sin$\alpha$ | $\mu_3$:0.5$l_{14}$cos$\alpha$ |
| Reconfigured link 2-tip | -$l_{47}$ sin$\beta$ | $l_{47}$ cos$\beta$ |
| Reconfigured link 2-CM | -0.5 $l_{47}$ sin$\beta$ | 0.5 $l_{47}$ cos$\beta$ |

(SP) can be nullified by adopting high values of the corresponding *C* and *R* elements. Transformer moduli are represented as MTF (modulated transformer moduli).

Let now discuss how the net force acts on the manipulator. Let $X_v$ and $Y_v$ denote the body-fixed coordinates and the modeling of space robot is done in a non-inertial frame. The base of robot rotates about *Z*-axis. For a planar case, where, $\omega_x$ = 0, $\omega_y$ = 0 and $v_z$ = 0, the net force acting on manipulator can be given as (Merzouki et al. 2013; Pathak et al. 2006; Kumar et al. 2011)

$$F_x = M_V \ddot{x}_{CM} - M_V \dot{\phi} \dot{y}_{CM}, \tag{21}$$

$$F_y = M_V \ddot{y}_{CM} + M_V \dot{\phi} \dot{x}_{CM}, \tag{22}$$

$$F_z = 0. \tag{23}$$

Here, $M_v$ is the mass of the vehicle (robot base) and $\phi$ is the attitude or orientation of the space manipulator base.

The role of the Jacobian in velocity transformation and the PD controllers for joint control and the PID controllers for end-effector pose control are explained in the subsequent sub-sections.

### 2.1. Mapping of Joint Velocity into Cartesian Velocity

Jacobian maps the joint velocity into tip velocity. It is represented in figure 4 in the signal form (Kumar et al. 2013). The gains required to model Jacobian can be found from Equations 19 and 20 as,

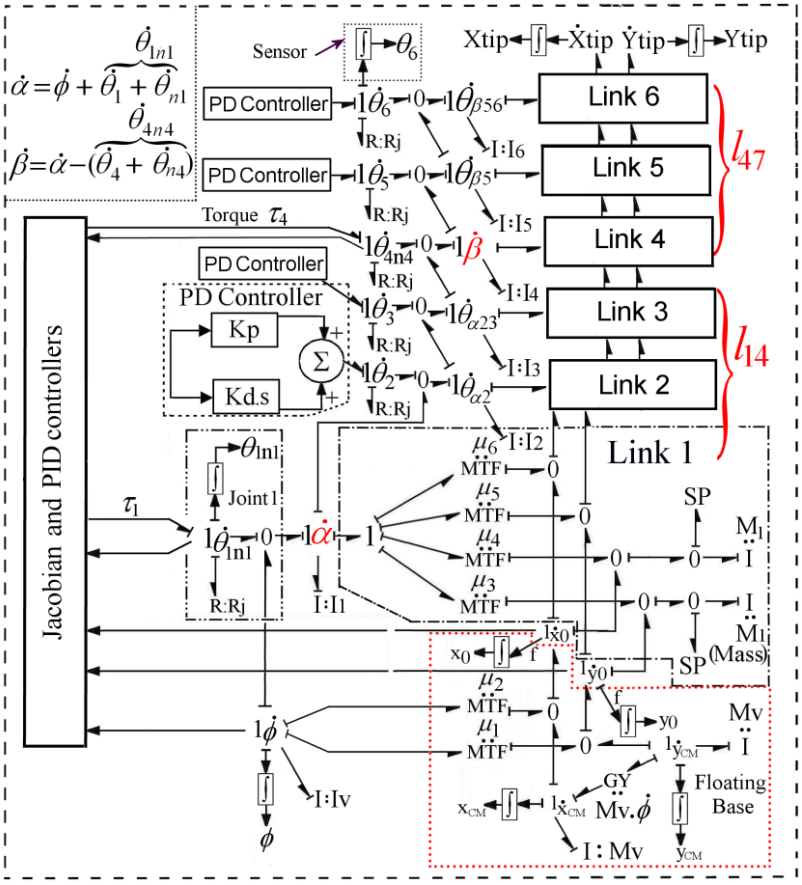


Figure 3: Bond Graph Model of 6 Links Space Robot System

$$\begin{bmatrix} \dot{X}_{tip}^{\#} \\ \dot{Y}_{tip}^{\#} \end{bmatrix} = \begin{bmatrix} \dot{X}_{CM} - r\dot{\phi}s\phi \\ \dot{Y}_{CM} + r\dot{\phi}c\phi \end{bmatrix} + \begin{bmatrix} -l_{14}s(\alpha) - l_{47}s(\beta) & -l_{47}s(\beta) \\ l_{14}c(\alpha) + l_{47}c(\beta) & l_{47}c(\beta) \end{bmatrix} \begin{bmatrix} \dot{\alpha} \\ \dot{\beta} \end{bmatrix} + \begin{bmatrix} -l_{14}s(\alpha) - l_{47}s(\beta) \\ l_{14}c(\alpha) + l_{47}c(\beta) \end{bmatrix} \begin{bmatrix} \dot{\phi} \end{bmatrix} \quad (24)$$

The above Equation 24 can be rewritten in compact form as,

$$\begin{bmatrix} \dot{X}_{tip} \\ \dot{Y}_{tip} \end{bmatrix} = \begin{bmatrix} \dot{X}_{CM} + \dot{\phi}\mu_2 \\ \dot{Y}_{CM} + \dot{\phi}\mu_1 \end{bmatrix} + \begin{bmatrix} K_3 & K_1 \\ K_4 & K_2 \end{bmatrix} \begin{bmatrix} \dot{\alpha} \\ \dot{\beta} \end{bmatrix} + \begin{bmatrix} K_5 \\ K_6 \end{bmatrix} \begin{bmatrix} \dot{\phi} \end{bmatrix} \quad (25)$$

Where, gains $K_1$, $K_2$, $K_3$, $K_4$, $K_5$ and $K_6$ are used for the Jacobian of the space robot.

### 2.2. PD Controllers

PD controllers are used herein at each joint to control the joint motion, i.e., to make joints active and passive. As shown in Figure 3, initially joints 1 and 4 are made active while others are kept passive. The actuated (active) joints are regulated by the PID controllers. Redundancy of the proposed robot system facilitates to choose joint as active/passive as per requirement. To control joint motion, PD control is used as shown in Fig. 4. The control law for the actuator at the joint is given as,

$$\tau = K_p(\theta_d - \theta_a) - K_d\dot{\theta}_a \quad (26)$$

Where, $\tau$ is the joint torque, $\theta_d$ is the desired position of joint and $\theta_a$ is the actual position of joint, $\dot{\theta}_a$ is the actual joint angular velocity. $K_p$ and $K_d$ are the proportional and the derivative gain parameters, respectively.

### 2.3. PID Controllers

PID controllers are used herewith in $X$ and $Y$ tip of the space robot as shown in figure 4. The aim of using it is to compare the actual velocity signal to the reference velocity signal and to correct it in case of error presence. The corrected signals are then sent to the each actuated joint of the manipulator through the Jacobian. Hence, one can get a close trajectory tracking during the task. The PID controllers are represented in the form of signal block diagrams in figure 4. In these block diagrams, $K_p$, $K_i$ and $K_d$ represent proportional gain, integral gain and derivative gain, respectively. $\dot{X}_{tip}$ and $\dot{Y}_{tip}$ are the actual velocity signals and $\dot{X}_{ref}$ and $\dot{Y}_{ref}$ are the reference velocity signals in $X$ and $Y$ directions, respectively. $\delta x$ and $\delta y$ are the trajectory error in $X$ and $Y$ directions, respectively.

## 3. RECOGNITION OF OBSTACLES

The obstacles present in the workspace are recognized by providing a barrier encircling the obstacles as shown in Figure 5. Assuming that obstacle 1 has a hexagonal shape and obstacle 2 is of a square shaped. The mathematical expression for obstacle detection (Mu et al. 2014; Shari and Troch 1996) can be given as,

$$d_{iLO} = f(x_i, y_i) \quad (27)$$

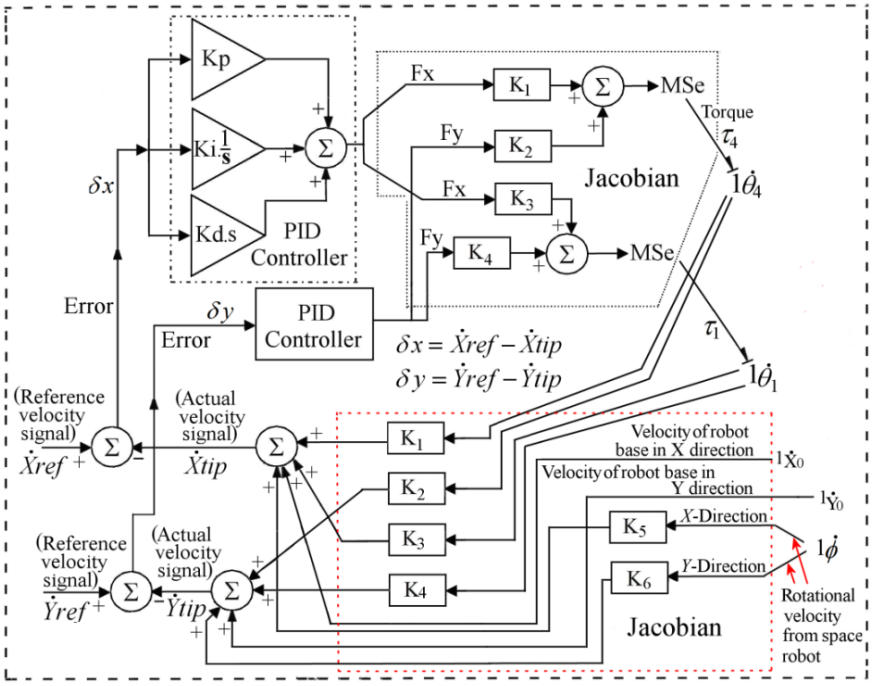


Figure 4. Jacobian and PID Controllers Interfacing with Space Robot System.

Where, $d_{iLO}$ denotes the pseudo-distance between the manipulator link and $i$ number of the obstacles.

and, $f(x_i, y_i) = (x_i - x_{ci})^2 + (y_i - y_{ci})^2 - a_i^2$ (28)

The co-ordinates, $x_i$ and $y_i$ represent the tip position near the obstacles. The co-ordinates $x_{ci}$ and $y_{ci}$ are the centre of mass coordinates of the obstacles's barrier and $a_i$ is the radius of the barrier.

If, $d_{iLO} > 0$, there is no collision

$= 0$, there is possibility of collision

$< 0$, there is possibility of serious collision.

To avoid obstacles, we need to maintain $d_{iLO}>0$. This condition can be satisfied completely by arresting the tip motions when it comes close to the obstacles. This can be done through locking the respective or influencing joint variable. Then, one of the passive joints needs to be made active simultaneously and hence the robot needs to be reconfigured to continue the desired motion planning. Now the question may arise that at what positive value of the pseudo-distance, the robot need to be reconfigured. This should be done at a minimum positive value of the pseudo-distance. However, it's as much as positive value can provide safest motion planning.

This concept can be extended for the proposed robot system as follows:

Stage I: This stage is schematically represented in Figure 5. The circumstance when both the obstacles collide with the manipulator is shown in this figure. Let's divide the whole manipulator into two sections for simplicity as shown in figure 5. In the first section of the manipulator only joint 1 is active and in the second section, only joint 4 is active. At this stage, let we get $d_{1LO} < 0$ for obstacle 1 and $d_{2LO} < 0$ for obstacle 2 in section 1 and 2 of the manipulator, respectively. These mean that the robot system suffers a serious collision from both the obstacles.

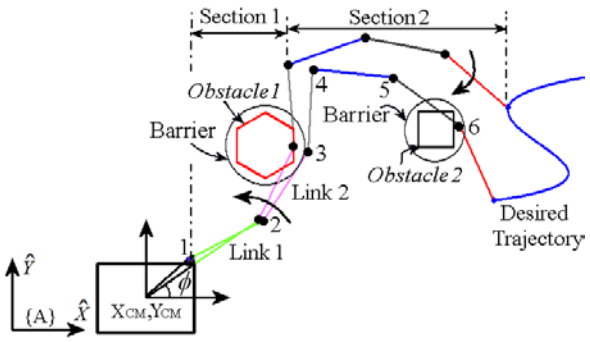


Figure 5: Stage I

Let us now assume that the space robot system avoids both the obstacles one by one.

Stage II: This stage is schematically represented in Figure 6. This figure shows the circumstance (assuming) when the robot avoids obstacle 1 but unable to avoid obstacle 2. Let us now discuss the occurrence of this situation. Suppose link 2 tip comes close to the obstacle 1 during the task. If it continues, first section of the manipulator will collide to the obstacle 1. To avoid this collision, let joint 1 is made passive during manipulation at minimum positive value of $d_{1LO}$ ensuring safe margin between the barrier and the surrounding links. This act will restrict motion of its influencing link tip, i.e., tip of link 2 as joints 2 and 3 are already passive. At this moment, however, the first section of the manipulator will not collide to the obstacle 1 but the robot tip will not trace the designated path due to lacking of the necessary and required two active joints.

To avoid this problem let joint 6 is made active. Hence, joints 4 and 6 are now active. A selection of which joint to be actuated while manipulation depends upon instant manipulator's configuration ensuring collision free-trajectory. By doing this, condition, i.e., $d_{1LO} > 0$ will be satisfied. But it does not guarantee about the avoidance of manipulator from the obstacle 2. This means that $d_{2LO} < 0$. At this stage, only one condition is satisfied while the other is not satisfied. For, a collision-free trajectory both conditions must be fully satisfied. This will be addressed in stage III.

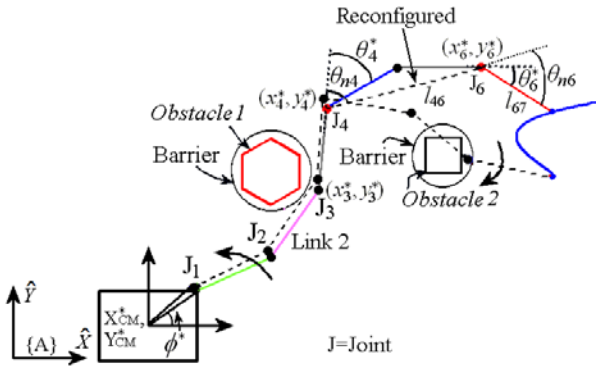


Figure 6: Stage II

The tip displacement expressions can be given as,

$$X^*_{tip} = X^*_{CM} + rc(\phi^*) + l_1 c(\theta_{(\phi 1)^*}) + l_2 c(\theta_{(\phi 12)^*}) + l_3 c(\theta_{(\phi 123)^*}) + l_{46} c(\alpha^*) + l_{67} c(\beta^*) \quad (29)$$

$$Y^*_{tip} = Y^*_{CM} + rs(\phi^*) + l_1 s(\theta_{(\phi 1)^*}) + l_2 s(\theta_{(\phi 12)^*}) + l_3 s(\theta_{(\phi 123)^*}) + l_{46} s(\alpha^*) + l_{67} s(\beta^*) \quad (30)$$

$$\alpha^* = \theta^*_{\phi 123} - \theta_{n4}, \beta^* = \alpha^* - \theta_{n6}$$

$$\text{Where, } l_{46} = \sqrt{(x^*_6 - x^*_4)^2 + (y^*_6 - y^*_4)^2}, \quad l_{67} = \sqrt{(x^*_7 - x^*_6)^2 + (y^*_7 - y^*_6)^2} \quad (31)$$

It is notable that the superscript "*" with variables denotes the parameter's values at $d_{1LO} > 0$ and $t$ = 9s, are known by the sensors used in model as shown in Figure 3. The joint variables $\alpha^*$ and $\beta^*$ of the reconfigured robot can be evaluated in the same way as Equations 15 to 18.

Stage III: This stage is schematically represented in Figure 7. The circumstance when the manipulator could avoid both the obstacles is shown in this figure. Now to satisfy both the conditions as discussed in stage II, let joint 4 is made passive and joint 1 is again resumed which was locked in stage II. Hence, joints 1 and 6 are now active. Now problem may arise by selecting the joint 1 again as active (which was active in stage I and then made passive in stage II) if it causes collision of the manipulator's first section with the obstacle 1. To resolve this problem, one must always be assure that $d_{1LO} > 0$ and motion of the manipulator's first section must be away from that obstacle. If not then one must select other joint as active imparting complete collision-free trajectory.

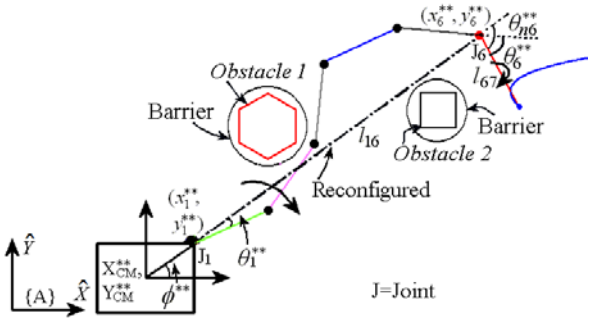


Figure 7: Stage III

The tip displacement expressions can be given as,

$$X_{tip}^{**} = X_{CM}^{**} + rc(\phi^{**}) + l_{16}c(\alpha^{**}) + l_{67}c(\beta^{**}) \quad (32)$$

$$Y_{tip}^{**} = Y_{CM}^{**} + rs(\phi^{**}) + l_{16}s(\alpha^{**}) + l_{67}s(\beta^{**}) \quad (33)$$

$$\alpha^{**} = \phi^{**} - \theta_1^{**}, \beta^* = \alpha^* - \theta_{n6}^{**},$$

Where, $l_{16} = \sqrt{(x_6^{**} - x_1^{**})^2 + (y_6^{**} - y_1^{**})^2}$, (34)

$$l_{67} = \sqrt{(x_7^{**} - x_6^{**})^2 + (y_7^{**} - y_6^{**})^2}.$$

$\alpha^{**}$ and $\beta^{**}$ of equations 32 and 33 can be found in the similar way as equations 15 to 18. Here, variables with superscript "**" are their values at $d_{1LO}, d_{2LO} > 0$ and $t$ = 17.5 s.

The Jacobian for stages I and II, can be evaluated in the same fashion as mentioned in section 3 and bond graph model can be drawn for the same.

How to choose which joint to be actuated can be decided by adopting optimization criterion such as energy optimum, smooth trajectory, etc. It is also worth mentioning that the obstacle avoidance as discussed above can be performed in a single attempt too. However, it is presented in three stages for better understanding and simplicity.

## 4. SIMULATION AND ANIMATION RESULTS

The proposed collision-free avoidance strategy has been considered to be validated through simulation and animation results. The bond graph model of the system equation has been implemented by the Symbol Shakti software (Mukherjee A. 2006). The simulation is carried out for 60 seconds. The input parameters used for simulation study are shown in Table 2.

Table 2: Input Parameters and their Value

| Robot Base and Link Parameters | | |
|---|---|---|
| Space Robot Base Mass ($M_v$)( kg ) | | 200 |
| Rotary Inertia of Base ($I_v$) (kg m$^2$) | | 40 |
| Location of Base of Arm from Vehicle CM ($r$)(m) | | 0.5 |
| Length of each Link | | 0.5 |
| Mass of each Link with Actuator (kg) | | 1 |
| Rotary Inertia of each Link (kg m$^2$) | | 0.5 |
| Pad Parameters | | |
| Stiffness of Spring ($K_s$) (Nm/rad) | | $5\times10^4$ |
| Stiffness of Spring ($K_h$)( Nm/rad) | | $3\times10^4$ |
| Damping Resistance ($R_d$)(Nms/rad) | | $1\times10^4$ |
| PID Gain Parameters | | PD Gain Parameters |
| Proportional Gain ($K_p$) | 3000 | $5\times10^4$ |
| Integrative Gain ($K_i$) | 2500 | - |
| Derivative Gain ($K_d$) | 2000 | $5\times10^4$ |
| Reference Trajectory: Control Points (m) | | |
| $p_{x0}$=2.892, $p_{y0}$ =1.115 , $p_{x1}$=1.572, $p_{y1}$=0.8822, $p_{x2}$=3.655, $p_{y2}$ = 0.54 , $p_{x3}$= 2.35, $p_{y3}$= 0.3674. | | |
| Obstacle Parameters | | |
| | Obstacle 1 | Obstacle 2 |
| Length of side (m) | 0.2 | 0.15 |
| CM Coordinates from Absolute Frame{$A$} (m) | $x_{c1}$ = 0.90<br>$y_{c1}$ = 0.72 | $x_{c2}$ = 2.0<br>$y_{c2}$ = 0.15 |
| Radius of barrier (m) | $a_1$ = 0.24 | $a_2$ = 0.21 |

Initial configuration of the space manipulator is given by the following joint coordinates in all cases:

$$\theta = \begin{bmatrix} 0 & 10^\circ & 30^\circ & 30^\circ & -30^\circ & -30^\circ & -30^\circ \end{bmatrix}$$

As a reference tip trajectory input, a B-spline curve of "*S*" shaped tip trajectory is taken. Let a B-spline curve with four control points (polynomial's third degree) is constructed for tip trajectory tracking. The reference tip displacement and velocity equations are as,

$$X_{tip} = p_{x0}(1-t/t_f)^3 + 3p_{x1}(t/t_f)(1-t/t_f)^2 + 3p_{x2}(t/t_f)^2(1-t/t_f) + p_{x3}(t/t_f)^3 \quad (35)$$

$$Y_{tip} = p_{y0}(1-t/t_f)^3 + 3p_{y1}(t/t_f)(1-t/t_f)^2 + 3p_{y2}(t/t_f)^2(1-t/t_f) + p_{y3}(t/t_f)^3 \quad (36)$$

$$\dot{X}_{tip} = [-3p_{x0}(1-t/t_f)^2 - 6p_{x1}(t/t_f)(1-t/t_f) + 3p_{x1}(1-t/t_f)^2 - 3p_{x2}(t/t_f)^2 + 6p_{x2}(t/t_f)(1-t/t_f) + 3p_{x3}(t/t_f)^2]1/t_f \quad (37)$$

$$\dot{Y}_{tip} = [-3p_{y0}(1-t/t_f)^2 - 6p_{y1}(t/t_f)(1-t/t_f) + 3p_{y1}(1-t/t_f)^2 - 3p_{y2}(t/t_f)^2 + 6p_{y2}(t/t_f)(1-t/t_f) + 3p_{y3}(t/t_f)^2]1/t_f \quad (38)$$

Where, ($p_{x0}$, $p_{y0}$) .. ($p_{x3}$, $p_{y3}$) are four control points of B-spline curve corresponding to *X* and *Y* directions and *t* is time and $t_f$ is final travel time.

Let us now discuss the simulation and the animation results.

### 4.1. Collision Recognition

To detect collisions, pseudo-distance (Mu et al. 2014) criterion has been used. Figure 8 shows the pseudo-distance between the manipulator and the obstacles during the task. Figure 8 (a) depicts the pseudo-distance for traditional trajectory planning (stage I). From this figure, one can observe that the pseudo-distance, $d_{1LO} < 0$ between the time interval of 12.6s and 17.1s. This is the period when the manipulator collides critically with the obstacle 1. Also, the pseudo-distance, $d_{2LO} < 0$ after $t$ = 58.7s. This means that the whole manipulator suffers a serious collision with the obstacle 2 after $t$ = 58.7s. Figure 8(b) exhibits the pseudo-distance for partial collision-free trajectory. From this figure, it is seen that the pseudo-distance, $d_{1LO} > 0$ throughout the manipulation. This means that the first section of the manipulator is now able to save itself from the obstacle 1. It is also seen that the pseudo-distance, $d_{2LO} < 0$ between the time interval of 25.7s and 54s which illustrates the serious collision of the manipulator's second section as discussed with the obstacle 2. Hence, from this figure one gets to know that the manipulator could avoid the obstacle 1 but not the obstacle 2. Figure 8(c) shows the pseudo-distance for complete collision-free trajectory. From this figure, it is seen that the pseudo-distance, $d_{1LO}$ and $d_{2LO} > 0$ throughout the manipulation. This means that the whole manipulator now completely avoids both the obstacles and provides complete collision-free trajectory.

### 4.2. Trajectory Planning

This sub-section deals about the simulation results of trajectory tracking planning in the presence of the obstacles in the workspace for all three stages as discussed.

Figure 9 shows the reference and the actual tip trajectory in the presence of the two obstacles in the workspace. Figure 9(a) depicts the tip trajectory when both the obstacles collide with the whole manipulator (stage I as discussed). This stage is expressed as traditional trajectory planning in (Mu et al. 2014). From figure 9 (a), it is observed that the tip closely follows the designated path. In this figure, 1,4A denotes that joints 1 and 4 are active joints. Figure 9(b) represents the tip trajectory when the manipulator avoids obstacle 1 but collides with obstacle 2 (stage II). This stage can be expressed as partial collision-free trajectory. From figure 9(b), it is seen that the robot closely track about half of the designated path but does not the rest half. This trajectory error occurs due to not to be sufficient torque generation by the active joints 4 and 6. This trajectory tracking is the resultant of the circumstance when the active joint 1 is made passive and the passive joint 6 is made active during manipulation. The joint 1 is made active to avoid collision to its influencing link and joint 6 is made active to keep continue the desired motion. Hence, joints 4 and 6 are now active which are denoted by 4,6A in figure 9(b). From this figure, close trajectory tracking is observed. Figure 9(c) shows the tip trajectory when the whole manipulator avoids both the obstacles completely (stage III). This stage can be expressed as complete collision-free trajectory. From this figure, one can see that the robot closely trace the given reference input. In this figure, other than1,4A, 4,6A represents that joints 4 and 6 are now active and 1,6A represents that joints 1 and 6 are then now active.

### 4.3. Joint Rotation

This sub-section gives information about which joint is whether actuated or not during the task. Figure 10 shows the joint rotation with respect to time. Figure 10(a), (b) and (c) represents the joint rotation for the three stages I, II and III, respectively, as discussed in sub-section 4.2. Figure 10(a) illustrates that only joints 1 and 4 are active, whereas others are passive. Figure 10(b) exhibits that joints 1 and 6 are made passive and active, respectively, at $t$ = 9s during the task. From figure 10(c), it is seen that joint 4 is made passive and instead of it, joint 1 is again made active at $t$ = 17.5s during the task. The reason behind making active/ passive to which joint and at what circumstances is well addressed in sub-section 4.2.

### 4.4. Animated View of Trajectory Planning

This sub-section discusses about the animation results. Animation is the other way of validation of the proposed work in addition to the simulation. Figure 11 shows the animated view of the trajectory planning as discussed in sub-section 4.2. Figure 11(a), (b) and (c) represents the animation results for the three stages I, II and III, respectively, as discussed in sub-section 4.2. From figure 11(a), it is seen that trajectory tracking is successfully accomplished but both the static obstacles collide with the space manipulator. From figure 11 (b), one can see that the manipulator is able to avoid obstacle 1 but at the same time it collides with the obstacle 2. From figure 11(c), it is illustrated that the manipulator is now able to avoid both the static obstacles during its tip trajectory.

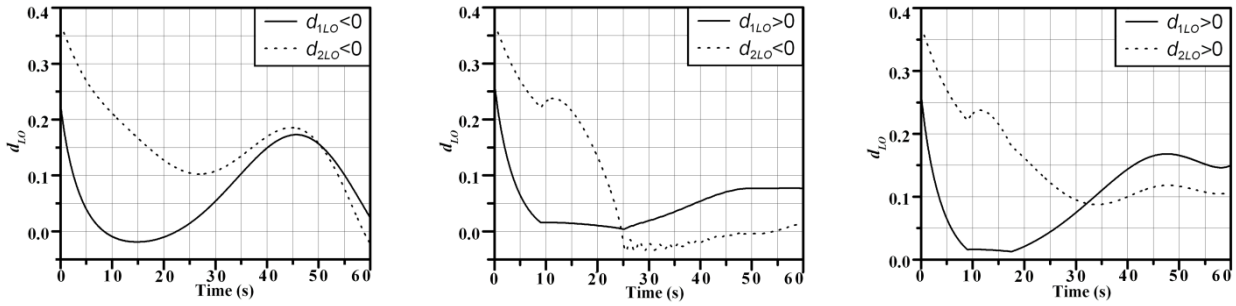


(a) (b) (c)

Figure 8: The pseudo-distance between the manipulator and the obstacles, (a) stage I (b) stage II and (c) stage III.

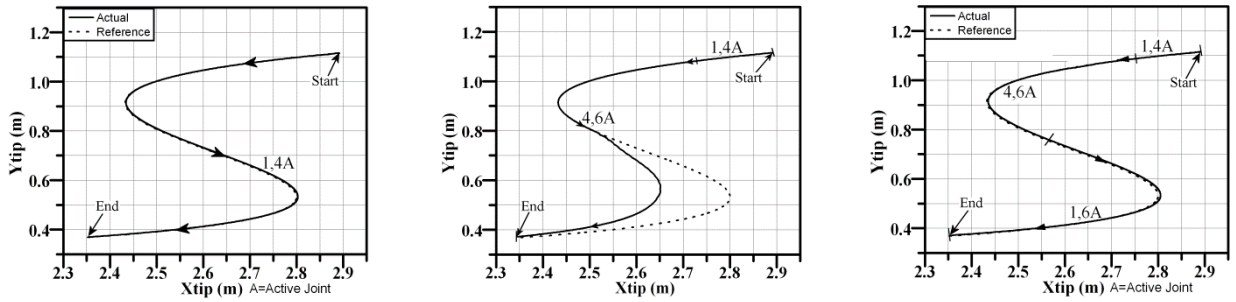


(a) (b) (c)

Figure 9: The tip trajectory tracking of the 6 links space robot system, (a) stage I (b) stage II and (c) stage III.

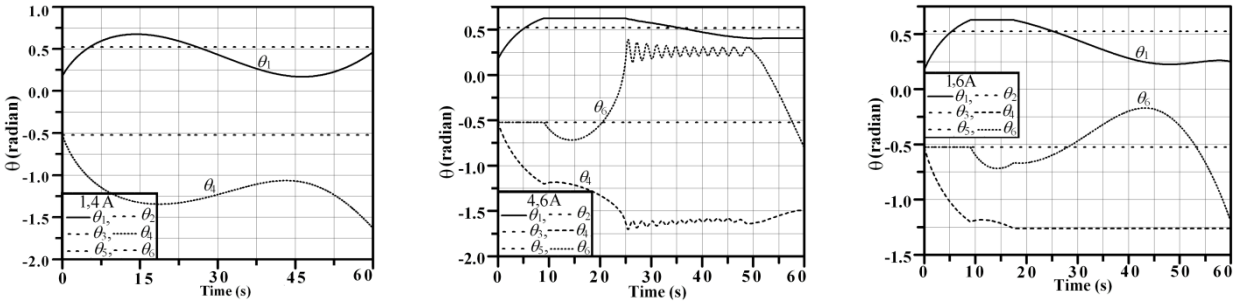


(a) (b) (c)

Figure 10: The joint rotation of the 6 links space robot system, (a) stage I (b) stage II and (c) stage III.

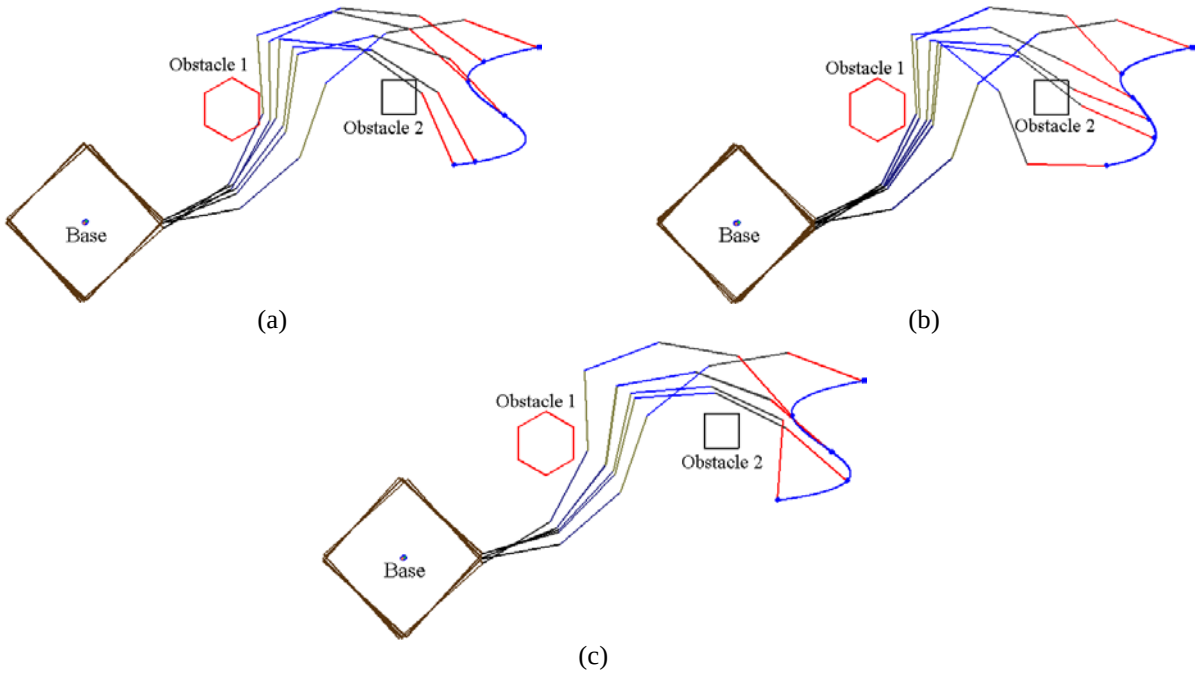


(a) (b)

(c)

Figure 11: Animated view of collision-free trajectory of the 6 links space robot, (a) stage I (b) stage II and (c) stage III.

## 5. CONCLUSION

Based on the reconfiguration approach, we proposed 6DOF space manipulator for obstacle avoidance during trajectory tracking in the presence of the two obstacles in the workspace. For the kinematic control purpose, only two joints are made active at a time during the task. Reconfigurations have been done after detection of the obstacles in the workspace based on the pseudo-distance criterion. Each joint is controlled by employing the PD controller, whereas for tip motion control, PID controllers have been used. The simulation and the animation results validated the successful execution of the proposed approach for collision-free trajectory planning. This work will be extended for dynamic obstacles in the workspace. Also, a practical 3-D collision-free trajectory planning will be done.

## REFERENCES


Agrawal O P and Xu Y, 1994. On the global optimum path planning for redundant space manipulators. IEEE Transactions on Systems, Manand Cybernetics 24(9): 1306-1316.

Bjerkeng M, Transeth A A, Pettersen K Y, Kyrkjebø E and Fjerdingen S A, 2011. Active Camera Control with Obstacle Avoidance for Remote Operations with Industrial Manipulators: Implementation and Experimental Results. IEEE/RSJ International Conference on Intelligent Robots and Systems (IROS), September 25-30, San Francisco, CA, USA.

Csiszar A, Drust M, Dietz T, Verl A and Brisan C, 2012. Dynamic and interactive path planning and collision avoidance for an industrial robot using artificial potential field based method. Mechatronics. Springer Berlin Heidelberg, 413-421.

Dassanayake P, Watanabe K and Izumi K, 1999. Fuzzy Behavior-Based Control for a Task of Three- Link Manipulator. Proceedingsof the 1999 IEEE International Conference on Systems, Man and Cyber, II-776-781, 12-15 October, Tokyo, Japan.

Klein C A and Huang C H, 1983. Review of pseudoinverse control for use with kinematically redundant manipulators. Systems, Man and Cybernetics, IEEE Transactions 13(3): 245-250.

Korayem M H, Nazemizadeh M and Rahimi H N, 2014. Dynamic optimal payload path planning of mobile manipulators among moving obstacles. Advanced Robotics 28.20: 1389-1402.

Koren Y, Borenstein J, 1999. Potential Field Methods and their Inherent Limitations for Mobile Robot Navigation. Proceedings of the IEEE International Conference on Robotics and Automation, 1398–1404, April 9–11, Sacramento, California.

Kumar A, Pathak P M, and Sukavanam N, 2011. Reduced model based control of two link flexible space robot. Intelligent Control and Automation, 2.02: 112.

Kumar V, and Pathak PM, 2013. A Stable Docking Operation by a Group of Space Robots. Proceedings of the 1st International and 16th National Conference on Machines and Mechanisms (iNaCoMM2013), IIT Roorkee, India, Dec. 18-20.

Mu Z, Xu W, Gao X, Xue L and Li C, 2014. Obstacles Modeling and Collision Detection of Space Robots for Performing On-Orbit Services. The 4th IEEE Conference on International Information Science and Technology (ICIST), 2014, 2014.

Mukherjee A, Karmarkar R and Samantray A K, 2006. Bond Graph in Modeling, Simulation and Fault Identification. New Delhi, I. K. International Publishing House Private. Limited.

Pathak P M, Mukherjee A and Dasgupta A, 2006. Attitude control of a free-flying space robot using a novel torque generation device. Simulation, 82.10: 661-677.

Pathak P M, Mukherjee A and Dasgupta A, 2006. Impedance control of space robot. International Journal of Modelling and Simulation, 26.4: 316.

R Merzouki, Samantaray A K, Pathak P M and Bouamam B O, 2013. Intelligent Mechatronic Systems: Modelling, Control and Diagnosis, Springer 2013.

Saha S K, 1996. A unified approach to space robot kinematics. Robotics and Automation, IEEE Transactions on 12.3: 401-405.

Sardana L, Sutar M K and Pathak P M, 2013. A geometric approach for inverse kinematics of a 4-link redundant in-vivo robot for biopsy. Robotics and Autonomous Systems 61.12: 1306-1313.

Shahri R N and Troch I, 1996. Collision-avoidance for redundant robots through control of the self-motion of the manipulator. Journal of Intelligent and Robotic Systems, 16.2: 123-149.

Singla E, Tripathi S, Rakesh V, Dasgupta B,2010. Dimensional synthesis of kinematically redundant serial manipulators for cluttered environments. Robotics and Autonomous Systems, 58.5: 585-595.

Sutar M K, Pathak P M, Mehta N K, Sharma, A K and Gupta V K, 2014. Inverse kinematics and control of 4-degree-of-freedom wire-actuated in vivo robot. Proceedings of the Institution of Mechanical Engineers, Part I: Journal of Systems and Control Engineering, 229: 77-91.

Whitney D E, 1969. Resolved motion rate control of manipulators and human prostheses. IEEE Transactions on Man-Machine Systems, MMS, 10(2), 47–53.



**Vijay Kumar Dalla** is a Ph.D. student at Robotics and Control Lab in the Department of Mechanical and Industrial Engineering, IIT Roorkee, India. He did Master of Technology (M.Tech.) from IIT Bombay in 2008. He did Bachelor of Engineering (B.E.) in Mechanical Engineering from Government Engineering College, Bilaspur, Chhattisgarh, India in 2006. His research area is a space robotics.

**Pushparaj Mani Pathak** received the B. Tech. degree in 1988 from NIT, Calicut, India and M. Tech. degree in 1998 from IIT, Kanpur, India both in Mechanical Engineering. He received Ph. D. degree in 2005 from IIT, Kharagpur,India. Currently he is an Associate Professor in the Department of Mechanical and Industrial Engineering, Indian Institute of Technology, Roorkee, India. His areas of interest are space robotics, walking robots, and dynamics and control.